Turbulence, Heat and Mass Transfer 7

Effects of Pressure Gradient on Higher Order Statistics in Turbulent Boundary Layers

Z. Harun[1], I. Marusic[2], J. P. Monty[3] and R. Mathis[4]

[1]*Department of Mechanical and Materials,*
The National University of Malaysia, 43600 Bangi, Malaysia, zambri@eng.ukm.my

[2]*Department of Mechanical Engineering, The University of Melbourne,*
Melbourne, VIC, 3010, Australia, imarusic@unimelb.edu.au

[3]*Department of Mechanical Engineering, The University of Melbourne,*
Melbourne, VIC, 3010, Australia, montyjp@unimelb.edu.au

[4]*Department of Mechanical Engineering, The University of Melbourne,*
Melbourne, VIC, 3010, Australia, rmathis@unimelb.edu.au

Abstract — This paper investigates the effect and influence of pressure gradient on the skewness and flatness in turbulent boundary layers, which are subjected to adverse, zero and favourable pressure gradients. The large scale features are found to increase the skewness in the near wall-region for adverse pressure gradients in a manner similar to the effect of changing Reynolds number as documented by Metzger & Klewicki [1] for zero pressure gradient flows. The skewness is expanded by decomposing the fluctuating velocities into small and large-scale components, $u^+ = u_L^+ + u_S^+$, and the individual terms are compared. The large-scale term, $\overline{u_L^{+3}}/\overline{(u^2)}^{3/2}$, and the cross product term, $\overline{3u_L^+ u_S^{+2}}/\overline{(u^2)}^{3/2}$, are found to be the major contributors for the skewness factors and change drastically with pressure gradient. Further, it is found that the cross product term could replace the amplitude modulation method proposed by Mathis *et al* (2009) [2] in turbulence boundary layer flows with pressure gradient.

1. Introduction

Studies of large-scale structures in wall-bounded shear flows have been successfully documented in recent years in pipe & channel flows and in the zero pressure gradient (ZPG) flow. Hutchins & Marusic (2007) [3] have shown that the large-scale motions influence the near-wall turbulence substantially, by mean of superposition and modulation effects. Mathis *et al* (2009) established a method to quantify the influence of the large-scale features of the outer region on the near-wall small-scale features in the form of an amplitude modulation. Furthermore, Marusic *et al* (2010) [4] compared a large range of Reynolds number $1000 < Re_\tau < 10^6$ and found these large-scale features to have a greater influence on the near-wall motions as the Reynolds numbers increase. Marusic *et al* (2010) showed that the large-scale features in the log region become increasingly important in sustaining and producing turbulence as compared with the small-scale features near the wall. The role of large-scale motions in turbulent boundary layers with pressure gradients is not as well documented. This is notwithstanding the recent studies in wall turbulence with pressure gradient flows by Lee & Sung (2009) [5], Dixit & Ramesh (2010) [6] and Rahgozar & Maciel (2011) [7], who highlighted the lack of such studies despite their strong relevance to engineering applications.

Nonetheless, there has been a lot of progress in identifying the effect of pressure gradients. Bradshaw (1967) [8] found that the inactive motions or the large-scale structures are more intense in a strong adverse pressure gradient flow. Lee & Sung (2009) and Rahgozar & Maciel (2011) found more large-scale features in stronger pressure gradient flows which resemble the large, streaky structures in ZPG flows (Hutchins and Marusic (2007) [9], Tomkins and Adrian (2003)

Table 1: Experimental parameters. f and T are the sampling frequency and duration, respectively.

Pressure Gradient	Symbols	x (m)	U_1 (m/s)	U_τ (m/s)	Re_τ	Re_θ	δ (m)	ν/U_τ (μm)	l^+	
APG	◇	4.0	20.0	0.645	3200	12030	0.077	24.6	30	
ZPG	□	2.9	20.9	0.739	3000	8920	0.065	20.5	30	
FPG	○	4.0	18.1	0.710	3100	6450	0.066	21.3	30	cont.

Pressure Gradient	Symbols	f (kHz)	TU_1/δ $\times 10^3$	β	K $\times 10^{-7}$
APG	◇	50	26.3	1.74	-1.05
ZPG	□	50	30.0	0	0
FPG	○	50	21.8	-0.42	0.77

[10]). Monty *et al* (2011) [11] found that the increased large-scale features are responsible for the rise in turbulence intensities both in the inner and outer regions. Harun *et al* (2011) [12] showed that the increased large-scale features due to mild APG may not cause any change in the near-wall streak spacing[1]. These preliminary studies are useful in characterising the flow structures, however these studies are limited. As suggested by Monty *et al* (2011) and Harun *et al* (2011), higher Reynolds number studies should be performed and analysed to confirm the results. Furthermore, higher order statistics analyses highlighting such effects appear to be lacking in the literature. This paper identifies the influences of the large-scale features based on information from higher order turbulence statistics which are the skewness and flatness factors at relatively high Reynolds number.

2. Experimental set up

2.1. Facility

The experiments were performed in an open-return blower wind tunnel. Detailed descriptions of the wind tunnel set-up are given in Monty *et al* (2011) and Harun (2012) [13]. Figure 1 shows the coefficient of pressure, C_p, plotted against streamwise position. The ZPG section spans for 3 m and the APG or FPG section starts from $x = 3$ m onwards (x is used for the streamwise direction and z is used for the wall-normal direction). The ceiling heights for the pressure gradient section is adjustable. The pressure gradient was carefully adjusted so that the C_p was set to be within ± 0.01 throughout the inlet velocities tested.

Oil Film Interferometry (OFI) was used to determine the skin friction coefficient, C_f. More details concerning the OFI method, background and calibration can be found in Harun (2012) and Chauhan *et al* (2010) [14]. It has been shown in Monty *et al* (2011) that C_f only agrees (with C_f obtained from the Clauser chart method) for the ZPG cases, however for stronger APG flows,

[1]The change in streak spacing observed in Lee & Sung (2009) could be due to the amplitude modulation of the large-scale features in the outer region. Two-point correlations pick up the larger envelope of the fluctuations in the outer region, and it was the larger envelope which causes the analysis to yield wider streak spacing (Harun *et al*, 2011).

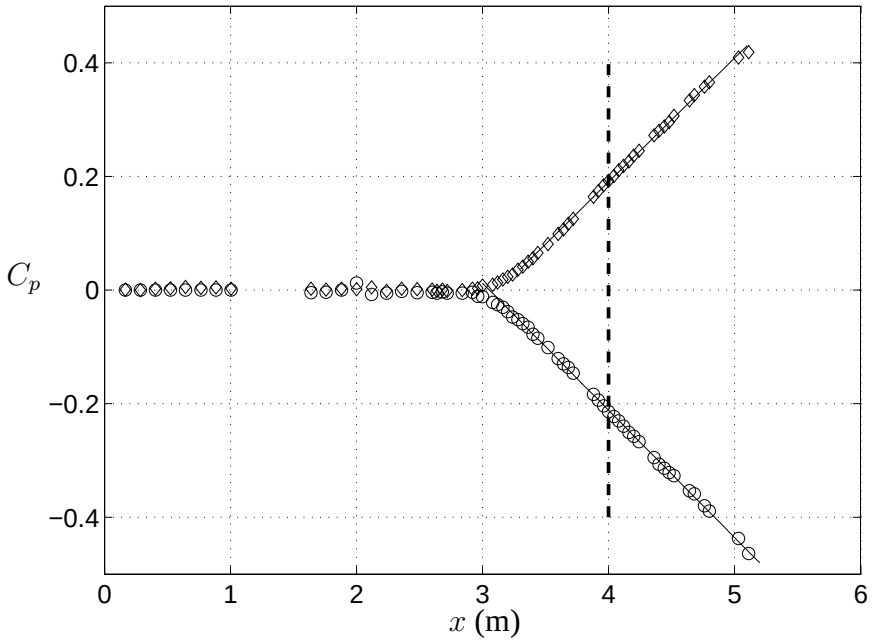

Figure 1: Pressure coefficient, C_p, for adverse pressure gradient ($\diamond$), and favourable pressure gradient ($\bigcirc$). Solid lines indicate a linear-fit of C_p and the vertical dashed-dotted line indicates the measurement location for data presented in this paper.

substantial deviation i.e. approximately 10% difference in C_f could be observed for $\beta \gtrsim 2.0$ (when compared with C_f obtained from the Clauser chart method). All friction velocities used for the analysis are calculated from the coefficient of frictions obtained from the OFI method.

2.2. Experimental parameters

All of the measurements were performed using single hot-wire anemometry. The hot-wire probes were all operated in constant temperature mode using an AA Lab Systems AN-1003 anemometer with overheat ratio of 1.8 and the system had a frequency response of at least 50 kHz. A Dantec probe support (55H20) was used. Wollaston wires of diameter ϕ = 2.5 μm were soldered to the prong tips and etched to give a platinum filament of the desired length, l. The dimensionless wire length was maintained constant ($l^+ = lU_\tau/\nu \approx 30$).

In Table 1, U_τ is the friction velocity. Superscript '+' is used to denote viscous scaling e.g. $z^+ = zU_\tau/\nu$ and $U^+ = U/U_\tau$. The friction Reynolds number, Re_τ, is given by $\delta U_\tau/\nu$, where δ is the boundary layer thickness determined from a modified Coles law of the wall/wake fit to the mean velocity profile (Jones *et al* (2001) [15]).

The adverse pressure gradient considered in this study is mild and the adverse pressure gradient parameter is represented by the Clauser (1954) [16] parameter

$$\beta = \frac{\delta^*}{\tau_o}\frac{dP}{dx}, \tag{1}$$

where δ^* is the displacement thickness and τ_o is the wall shear stress, P is the static pressure and x is the streamwise distance. The favourable pressure gradient is also mild and is represented by the acceleration parameter

$$K = \frac{\nu}{U_1^2}\frac{\mathrm{d}U_1}{dx}, \tag{2}$$

Table 2: Uncertainty estimates.

Source	Uncertainty
Pressure transducer	$\pm 0.15\%$
Temperature	$\pm 0.1\%$
Atmospheric pressure	$\pm 0.1\%$
Friction velocity, U_τ	$\pm 1\%$
Pitot probe uncertainty during calibration	$\pm 0.5\%$
Wire size, l	± 0.04 mm
Initial wall normal position	± 0.025 mm
Inner scaled mean velocity, U^+	$\pm \approx 2\%$
Inner scaled mean velocity, $\overline{u^2}^+$	$\pm \approx 4\%$

where U_1 is the local free-stream velocity. For the APG case, $\beta \approx 1.74$ and for the FPG case $K \approx 0.77 \times 10^7$. All experimental parameters are shown in Table 1.

2.3. Uncertainty estimates

Table 2 documents estimates of the experimental uncertainties. The method used in the uncertainty analysis is similar to the one in Kline and McClintock (1953) [17]. The hotwire uncertainties are consistent with findings from the well-calibrated hotwire study by Brunn (1995) [18]. The estimated errors are also consistent with recent experiments by Hultmark *et al* (2005) [19] and Ng *et al* (2011) [20].

The errors for friction velocity obtained from the OFI method is $\pm 1\%$. The accumulated errors for the mean velocity U^+ is $\pm 2\%$ arising from errors in skin friction, pressure transducer, temperature, atmospheric pressure and Pitot tube calibration. Hutchins *et al* (2009) [21] report that when spatial resolution is held constant by maintaining a constant inner-scaled wire length, the near-wall peak in turbulence intensity $\overline{u^2}^+|_m$ grows with the Reynolds number in ZPG flows. Later Chin *et al* (2009) [22] proposed that measurements made with $l^+ \approx 22$ result in 10% attenuation in $\overline{u^2}^+|_m$. Turbulence intensities $\overline{u^2}^+$ are not shown here, however the errors in turbulence intensities due to spatial resolution arising from $l^+ \approx 30$ is expected to be large in the near-wall region. The spatial resolutions in the skewness and flatness are expected to occur however these errors are consistent for constant l^+.

3. Results

This paper focuses only on the factors that contribute to the skewness and flatness of the streamwise fluctuating velocity. The skewness, S_u, and flatness, F_u, factors are defined as:

$$S_u = \frac{\overline{u^3}}{\overline{(u^2)}^{3/2}}, \qquad F_u = \frac{\overline{u^4}}{\overline{(u^2)}^2}. \tag{3}$$

The third moment of a turbulent statistic, such as $\overline{u^3}$ scaled by $\overline{(u^2)}^{3/2}$, describes the skewness, S_u, or asymmetry of the probability distribution of u. A symmetric pdf, such as a Gaussian function,

has $S_u = 0$. A positive value of S_u implies that large positive values of u are more frequent than large negative values. The fourth moment, or flatness, F_u, of the u distribution is given by $\overline{u^4}$ scaled with $\overline{(u^2)}^2$, and is a measure of the frequency of occurrence of events far from $u = 0$. If these are relatively frequent, F_u will take greater values than the Gaussian value of 3.

Figure $2(a)$ show the skewness of streamwise velocity fluctuations for adverse, zero and favourable pressure gradients at $Re_\tau \approx 3000$. A large difference between the three pressure gradient cases can be observed. The entire skewness profile is lifted up for the APG case and shifted down for the FPG case. For FPG, the skewness is negative, starting at $z/\delta = 0.008$ and remaining negative for the entire boundary layer. Skewness for APG remains positive from the near-wall region towards the wake region ($z/\delta \approx 0.3$), while skewness for the ZPG case is between the APG and FPG cases. The increased skewness coefficients in APG has been reported in Skåre & Krogstad (1994) [23] and Nagano & Houra (2002) [24] . The decrease of skewness coefficients in stronger FPG has also been reported, for example in Warnack & Fernholz (1998) [25].

Thus there is a difference in the skewness caused by the pressure gradient. It is important to note that here both non-dimensionalised sensor length, l^+, and friction Reynolds number have been matched between the cases. This is important as l^+ does cause differences in the near-wall region. Johannson & Alfredson (1983) [26] showed that skewness varied with sensor length i.e. $S_u \approx -0.2$ for $l^+ = 14$; however this changed to $S_u \approx 0$ for $l^+ = 32$ in the near-wall region ($20 \lesssim z^+ \lesssim 30$) at $Re_h \approx 50000$ in turbulent channel flow experiments (Re_h is Reynolds number based on channel height). Johannson & Alfredson (1983) compared two flows at relatively high but different Reynolds number, $Re_h \approx 50000$ and $Re_h \approx 129000$, at constant $l^+ = 33 - 34$, and showed that there was a slight difference in S_u. Therefore, the Reynolds number also does cause a difference in S_u. The current data was acquired at a constant Reynolds number and constant l^+, thus neither Reynolds number nor l^+ effects apply and the focus is solely on the differences due to pressure gradient.

In ZPG flows, Metzger & Klewicki (2001) demonstrated that it is the large-scale features that contribute to the rise of the skewness in the near-wall region. Monty *et al* (2011) showed that the large-scale features are energised with pressure gradients both in the near-wall and outer regions. Therefore the rise of the skewness in the near-wall region observed in Figure $2(a)$ is related to the increased large-scale features resulting from the APG. To confirm this, a high-pass filter was used to remove the large-scale features. The high-pass filter was the same as in Mathis *et al* (2009), where the cut-off for the filter was set at $\lambda_{xc} = \delta$ to ensure a sufficient separation of scales (Mathis *et al*, 2009, Monty *et al*, 2011).

Figure $2(b)$ show the skewness of the high-pass filtered data. It can be observed that the skewness profiles for all three cases are shifted down for the region $z^+ < 100$, which is similar to the observations in the study by Metzger & Klewicki (2001). Therefore it can be concluded that the APG flow contains more large-scale features or interactions involving large-scale features. The most distinguishing features of the high-pass filtered signal are located in the outer region. The difference in the outer region, at $z/\delta = 0.3$, is very large ($S_u \approx -0.15$ for APG and $S_u \approx -0.35$ for FPG). Interestingly, the filtered data show a closer resemblance to a Gaussian distribution ($S_u \approx 0$) for all three cases.

Figure $2(c)$ shows the flatness for all pressure gradient cases at $Re_\tau \approx 3000$. Noticeable differences can be observed between the cases, especially in the near-wall region ($z^+ \lesssim 50$) and much further out in the outer region, ($z/\delta \gtrsim 0.1$). In the near-wall region, the FPG case has the lowest value of F_u. The location at which the minimum of F_u occurs is approximately the same which is at $z^+ \approx 15$, similar to results by Warnack & Fernholz (1998). However, Warnack & Fernholz (1998) showed that the flatness for the FPG and ZPG cases are similar in the viscous region, which

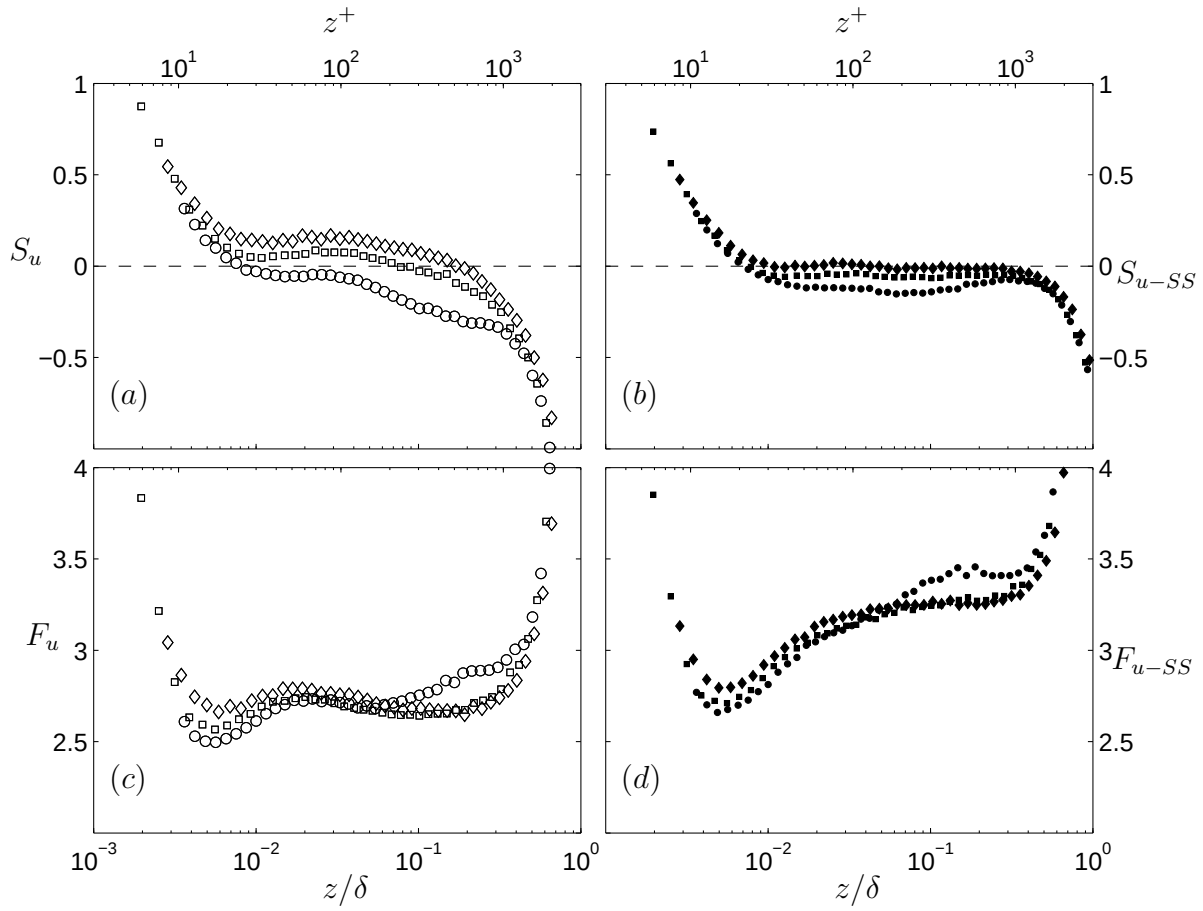

Figure 2: (a) Skewness S_u, (b) skewness for the high-pass filtered signal S_{u-SS}, subscript SS stands for small-scale, (c) flatness, F_u, and (d) flatness for the high-pass filtered signal F_{u-SS} for adverse, zero and favourable pressure gradients at $Re_\tau \approx 3000$. The skewness and flatness of the velocity fluctuations are denoted by open symbol ($\diamond$) APG, ($\square$) ZPG and ($\circ$) FPG. The high-pass filtered data are denoted by the closed symbols.

is not the case here. A difference of close to 5% can be seen between the FPG and ZPG cases and a difference of more than 8% can be observed between the FPG and APG cases. In the outer region, F_u coefficients for the ZPG and APG cases behave almost similarly. However, it should be noted that F_u coefficients for the APG case dip further than that for the ZPG case towards $z/\delta \approx 0.1$ to create another local minimum at $z/\delta \approx 0.2$. Therefore in the outer region, the APG has the smallest local minimum of F_u coefficients. It should be noted that the local minimum for the FPG case occurs much closer towards the wall. For the APG case, this result is in agreement with Nagano and Houra (2002.) Increased flatness with increasing FPG was also reported by Warnack & Fernholz (1998).

When the large-scale events are removed from the velocity fluctuations, F_u profiles for all cases are shifted up as shown in Figure $2(d)$. The shifts are greater in the outer region than in the viscous region. The results reflect that the large-scales reside in the outer region.

Metzger & Klewicki (2001) explained that a high-pass filter procedure systematically eliminates any additive effect of large-scale, low-frequency motions on measured statistics. In the near-wall

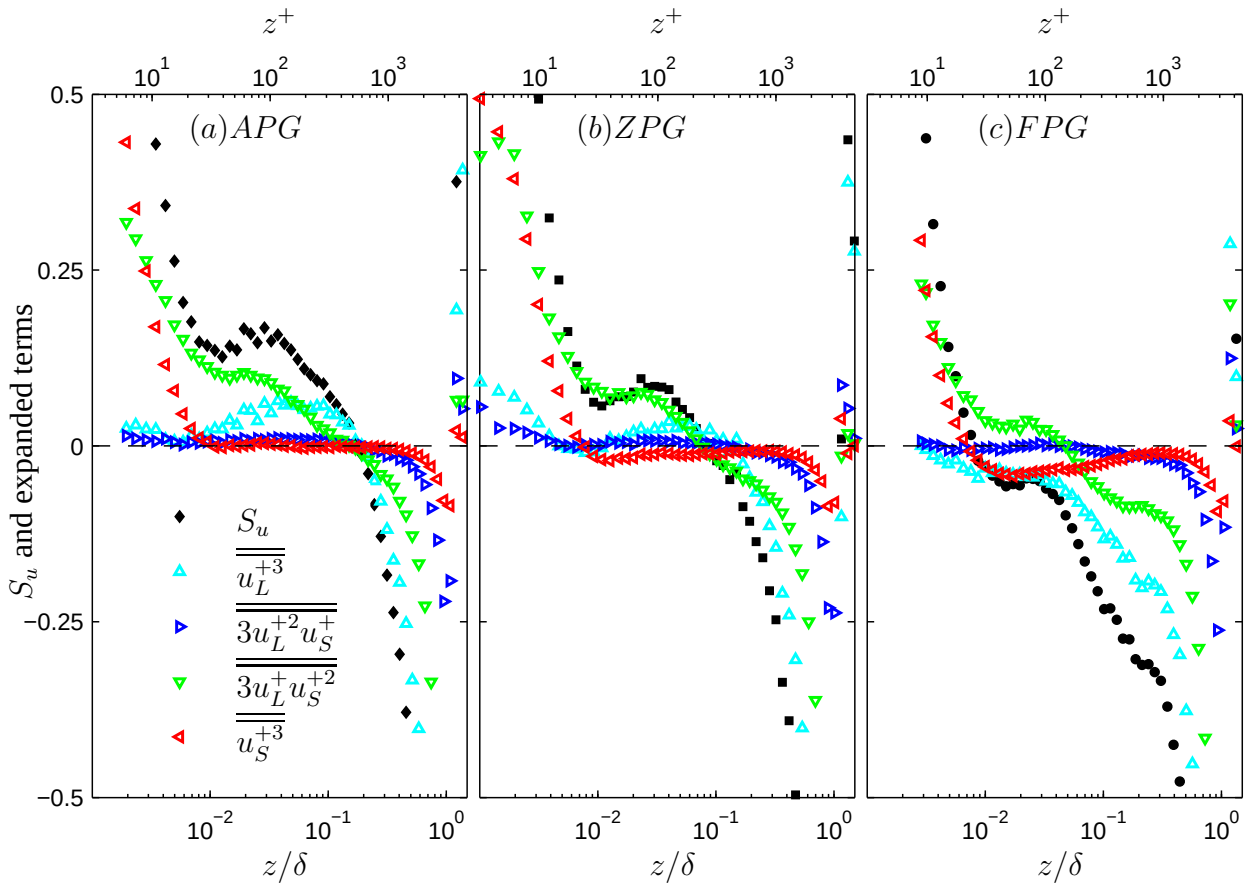

Figure 3: Skewness S_u for APG at $Re_\tau \approx 3000$. The skewness factors are expanded following $u^+ = u_L^+ + u_S^+$. The expanded terms are shown in (5).

region, this additive effect is prominent. However, in the outer region, small-scales co-exist among and within large-scales. A high-pass filter has a far-reaching effect when the large-scale components are removed. Therefore it is helpful to analyse the small and large-scale components and their contributions to these statistics. Following Schlatter & Örlü (2010) [27], Mathis *et al* (2011a) [28] expanded S_u using a decomposed signal such that $u^+ = u_L^+ + u_S^+$, where subscripts L and S denote the large- and small-scale components, therefore

$$S_u = \frac{\overline{u^{+3}}}{\left(\overline{u^{+2}}\right)^{3/2}} = \frac{\overline{u_L^{+3}} + \overline{3u_L^{+2}u_S^+} + \overline{3u_L^+u_S^{+2}} + \overline{u_S^{+3}}}{\left(\overline{u^{+2}}\right)^{3/2}}, \tag{4}$$

which can be simplified as

$$S_u = \overline{\overline{u_L^{+3}}} + \overline{\overline{3u_L^{+2}u_S^+}} + \overline{\overline{3u_L^+u_S^{+2}}} + \overline{\overline{u_S^{+3}}}, \tag{5}$$

where $\overline{\overline{ab}} = \overline{ab}/\left(\overline{u^{+2}}\right)^{3/2}$.

The skewness and each term of the decomposed skewness factors for all pressure gradient cases at $Re_\tau \approx 3000$ are shown in Figures $3(a)$, (b) and (c) for APG, ZPG and FPG flow respectively.

For all cases, it can be observed that the small-scales $\overline{\overline{u_S^{+3}}}$ contribute the most in the near-wall region up to $z^+ \approx 30$. It can also be observed that $\overline{\overline{u_S^{+3}}}$ contribution to S_u is similar for all cases. Therefore, pressure gradients do not cause the asymmetry of the probability distribution of u to change. Beyond $z^+ \approx 30$, the small-scales $\overline{\overline{u_S^{+3}}}$ for the APG case do not significantly contribute to the skewness until $z/\delta \approx 0.3$, where its contribution decreases rapidly. However, as the pressure gradient changes from APG to ZPG and FPG, there is a trend of negative contribution to the skewness in the region $30 \lesssim z^+ \lesssim 0.3\delta^+$.

The cross-term $\overline{\overline{3u_L^+u_S^{+2}}}$ seems to be the biggest contributor to the skewness for the entire boundary layer for all cases. The shape of S_u mostly adopts the trend in $\overline{\overline{3u_L^+u_S^{+2}}}$. The other cross-term $\overline{\overline{3u_L^{+2}u_S^+}}$ is the least significant term. For most of the region in the boundary layer, $\overline{\overline{3u_L^{+2}u_S^+}}$ has almost no contribution to the skewness.

The large-scale term $\overline{\overline{u_L^{+3}}}$ contribution to the skewness is increased from FPG to APG for the region $30 \lesssim z^+ \lesssim 0.3\delta^+$. For the entire boundary layer, $\overline{\overline{u_L^{+3}}}$ negatively contribute to the skewness, however in the ZPG and APG cases, $\overline{\overline{u_L^{+3}}}$ contributes positively to the skewness. From the terms $\overline{\overline{3u_L^+u_S^{+2}}}$ and $\overline{\overline{u_L^{+3}}}$, it can be concluded that pressure gradient causes the skewness to increase by increasing the contribution from the large-scale and cross-term.

Looking at each case separately, for the APG case, the small-scale term $\overline{\overline{u_S^{+3}}}$, and cross-term $\overline{\overline{3u_L^+u_S^{+2}}}$, appear to account for the majority of the S_u up to $z^+ \approx 30$. The large-scale term $\overline{\overline{u_L^{+3}}}$ becomes increasingly significant in region $30 \lesssim z^+ \lesssim \delta^+$. In the outer region, the rapidly vanishing values of cross-term $\overline{\overline{3u_L^+u_S^{+2}}}$ and large-scale term $\overline{\overline{u_L^{+3}}}$ are the majority contributor to the negative values in S_u. For the ZPG case, the small-scale term $\overline{\overline{u_S^{+3}}}$, and cross-term $\overline{\overline{3u_L^+u_S^{+2}}}$ are the significant contributors to S_u similar to the findings by Mathis *et al* (2011a). However, much smaller contribution from $\overline{\overline{3u_L^+u_S^{+2}}}$ is observed in the ZPG case when compared with the APG case.

Mathis *et al* (2011a) noticed that the $\overline{\overline{3u_L^+u_S^{+2}}}$ term is the most sensitive term to the increasing Reynolds number. The latter showed that if the $\overline{\overline{3u_L^+u_S^{+2}}}$ term was omitted, the reconstructed skewness without the $\overline{\overline{3u_L^+u_S^{+2}}}$ term was invariant over one order of magnitude in the Reynolds number. A modified skewness is given by $\tilde{S}_u$,

$$\tilde{S}_u = \overline{\overline{u_L^{+3}}} + \overline{\overline{3u_L^{+2}u_S^+}} + \overline{\overline{u_S^{+3}}}. \tag{6}$$

Figure 4 shows the reconstruction of the skewness without the cross product term , $\tilde{S}_u$. For the ZPG case, $\tilde{S}_u$ in the log region $40 \lesssim z^+ \lesssim 0.15Re_\tau$ approaches 0, which is similar to the results by Mathis *et al* (2011a). However, for the APG case, $\tilde{S}_u$ coefficients are larger. The additional contribution can be observed in Figure $3(a)$ to come from the term $\overline{\overline{u_S^{+3}}}$ for the region $z^+ \lesssim 30$ and from the term $\overline{\overline{u_L^{+3}}}$ in the log region $40 \lesssim z^+ \lesssim 0.15Re_\tau$. The larger contribution from $\overline{\overline{u_S^{+3}}}$ in the near-wall region and $\overline{\overline{u_L^{+3}}}$ in the outer region cause $\tilde{S}_u$ to take the shape of a plateau. $\tilde{S}_u$ coefficient for the FPG case is much smaller than the ZPG and APG cases. The deviations in $\tilde{S}_u$ across the pressure gradients cases suggest that the pressure gradient effects are not totally similar as in the effects of increasing Reynolds number. The pressure gradient effect seems to energise the large-scales (as in Reynolds number effects in ZPG), furthermore, there are also other effects

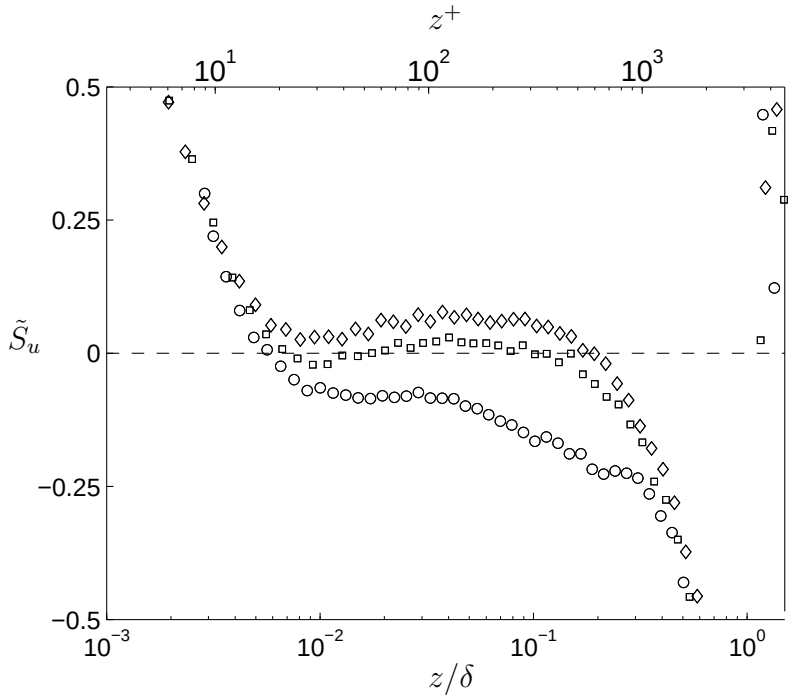

Figure 4: Skewness terms reconstruction without cross product term $\overline{\overline{3u_L^+u_S^{+2}}}$ (6) for APG, ZPG and FPG flows at matched $Re_\tau \approx 3000$. Symbol: ($\diamond$) APG, ($\square$) ZPG and ($\bigcirc$) FPG.

(such as increased $\overline{\overline{u_S^{+3}}}$ in the near-wall region and $\overline{\overline{u_L^{+3}}}$ in the log region discussed above) which need further studies.

The increased $\overline{\overline{u_S^{+3}}}$ and $\overline{\overline{u_L^{+3}}}$ in APG suggest that both small- and large-scale components are more active in APG. This is in agreement with Monty *et al* (2011) who observed increased contributions from both components in APG, resulting in larger turbulence intensities throughout the boundary layer.

Mathis *et al* (2011b) [29] and Schlatter & Örlü (2010) both linked their calculated amplitude modulation coefficients with the skewness coefficients and found an intimate relationship between the two statistics. Mathis *et al* (2011b) further presented that, with a correct multiplier, AM coefficients resemble the cross-term $\overline{\overline{3u_L^+u_S^{+2}}}$ over a wide range of Reynolds numbers $2800 < Re_\tau < 19000$. Figure $5(a)$ displays the cross product term $\overline{\overline{3u_L^+u_S^{+2}}}$ (open symbols) and AM (closed symbols) for APG, ZPG and FPG at $Re_\tau \approx 3000$.

From Figure 5, it should be noted that the cross product term $\overline{\overline{3u_L^+u_S^{+2}}}$ is larger for APG than for ZPG and FPG. This is related to the more energised large-scales in the near-wall region as the boundary layer is exposed to APG (Krogstad & Skåre, 1995, [30] Lee & Sung, 2009, and Monty *et al*, 2011). In the near-wall region, there is a high degree of modulation decreasing toward zero in the log-region and becoming negative in the wake region. In ZPG flow, as the Reynolds number increases, the large-scales become energetic and consequently increase the AM coefficients (Mathis *et al*, 2009). Likewise, APG strengthened the large-scales and the opposite effects occur due to APG. The zero-crossing or highly modulated region for the FPG case is smaller than the ZPG case and followed by the APG case.

It is interesting to observe that the zero crossing for the cross product term and AM occur at the same location for a particular pressure gradient case. This suggests that there could be a

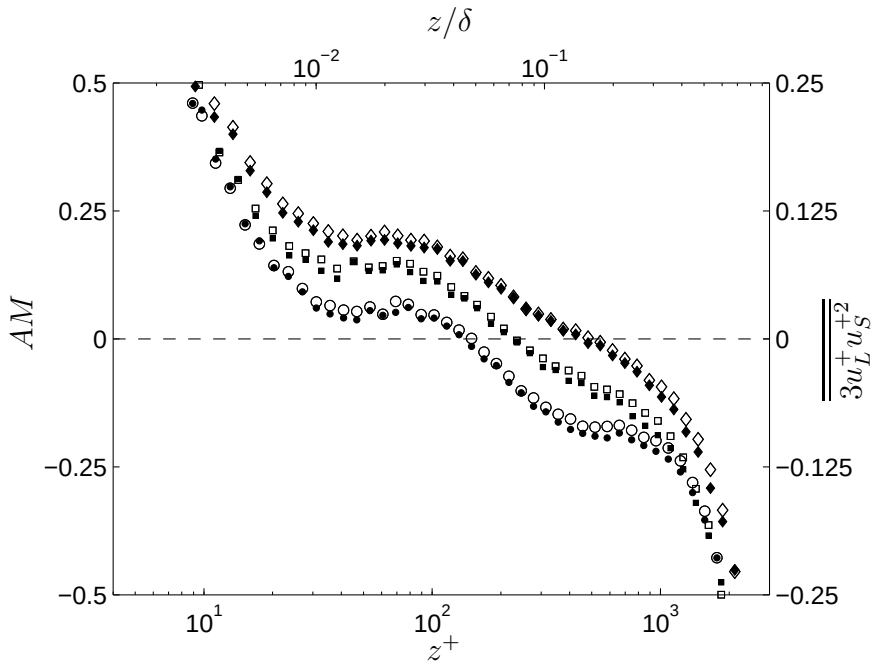

Figure 5: The relationship between the skewness cross-term $\overline{\overline{3u_L^+u_S^{+2}}}$ and amplitude modulation AM coefficients (Mathis *et al*, 2009) for APG, ZPG and FPG flows at matched $Re_\tau \approx 3000$. Symbol: ($\diamond$) APG, ($\square$) ZPG and ($\bigcirc$) FPG for $\overline{\overline{3u_L^+u_S^{+2}}}$ and closed symbols for AM coefficients.

relationship between the two statistics. The zero-crossing or highly modulated region for the FPG case is smaller (closer to the wall) than the ZPG case and followed by the APG case. A multiplier of 2 for the cross product term $\overline{\overline{3u_L^+u_S^{+2}}}$ appears to collapse both statistics within acceptable deviations as shown in Figure 5. As proposed by Mathis *et al* (2011a) the cross product term $\overline{\overline{3u_L^+u_S^{+2}}}$ could be an alternative or complimentary to the amplitude modulation and its robustness is proven over a wide range of Reynolds number. Here, we confirm the robustness for boundary layers with pressure gradients.

4. Conclusions

A set of experiments have been carried out to analyse the effect of pressure gradients on the skewness and flatness of the streamwise fluctuations velocity. In conclusion:

1. The removal of the large-scales from the velocity fluctuations causes the skewness coefficients to decrease and in contrast such removal causes the flatness coefficient to increase. These results reflect the pressure gradient effect, which increases the skewness coefficients and decreases the flatness coefficient (in the near-wall region) in APG.

2. The large-scale term, $\overline{u_L^{+3}}/\overline{(u^2)}^{3/2}$, and the cross product term, $\overline{3u_L^+u_S^{+2}}/\overline{(u^2)}^{3/2}$, are the major contributors to the skewness coefficients. These terms change rapidly with pressure gradients. The effects here shows that the large-scales and the large-scales interaction with the small-scales play major roles when pressure gradient changes.

3. The small-scale term $\overline{\overline{u_S^{+3}}}$ contribution to S_u do not seem to be affected by the changing pressure gradient term. This could be an indication that the features in the near-wall region

are not directly affected by pressure gradient. Rather the large-scales in the outer region influences and their interactions with the small-scales are the ones responsible for the change in S_u.

4. The cross product term, $\overline{u_L^+ u_S^{+2}}/\overline{(u^2)}^{3/2}$ could be used as an alternative to quantify the level of amplitude modulation proposed by Mathis *et al* (2009).

Acknowledgments
The authors are grateful for the financial support of the Australian Research Council.

References

1. M. M. Metzger and J. C. Klewicki. A comparative study of near-wall turbulence in high and low Reynolds number boundary layers. *Phys. Fluids*, 13:3, 692–701, 2001.
2. R. Mathis, N. Hutchins, and I. Marusic. Large-scale amplitude modulation of the small-scale structures in turbulent boudary layers. *J. Fluid Mech.*, 628:311–337, 2009.
3. N. Hutchins and I. Marusic. Large-scale influences in near-wall turbulence. *Phil. Trans. R. Soc. A*, 365:647–664, 2007.
4. I. Marusic, R. Mathis, and N. Hutchins. High Reynolds number effects in wall turbulence. *Int. J. Heat Fluid Flow*, 31:418–428, 2010.
5. J. H. Lee and H. J. Sung. Structures in turbulent boundary layers subjected to adverse pressure gradients. *J. Fluid Mech.*, 639:101–131, 2009.
6. Shivsai Ajit Dixit and O. N. Ramesh. Large-scale structures in turbulent and reverse-transitional sink flow boundary layers. *J. Fluid Mech.*, 649:233–273, 2010.
7. S. Rahgozar and Y. Maciel. Low- and high-speed structures in the outer region of an adverse-pressure-gradient turbulent boundary layer. *Exp. Thermal and Fluid Sci.*, 35:1575–1587, 2011.
8. P. Bradshaw. The turbulence structure of equilibrium boundary layers. *J. Fluid Mech.*, 29:625–645, 1967.
9. N. Hutchins and I. Marusic. Evidence of very long meandering features in the logarithmic region of turbulent boundary layers. *J. Fluid Mech.*, 579:1–28, 2007.
10. C. D. Tomkins and R. J. Adrian. Spanwise structure and scale growth in turbulent boundary layers. *J. Fluid Mech.*, 490:37–74, 2003.
11. J. P. Monty, Z. Harun, and I. Marusic. A parametric study of adverse pressure gradient turbulent boundary layers. *Int. J. Heat Fluid Flow*, 32:575–585, 2011.
12. Z. Harun, J.P. Monty, and I. Marusic. The structure of zero, favorable and adverse pressure gradient turbulent boundary layers. *In Proc. 7^{th} Turbulence and Shear Flow Phenomena, (TSFP). Ottawa, Canada*, 2011.
13. Z. Harun. *The structure of adverse and favourable pressure gradient turbulent boundary layers*. PhD thesis, University of Melbourne, Parkville, 2012.
14. K. Chauhan, H. C. H. Ng, and I. Marusic. Empirical mode decomposition and Hilbert transforms for analysis of oil-film interferograms. *Meas. Sci. Technol.*, 21:105405, 1–13, 2010.
15. M. B. Jones, I. Marusic, and A. E. Perry. Evolution and structure of sink flow turbulent boundary layer. *J. Fluid Mech.*, 428:1–27, 2001.
16. F. H. Clauser. Turbulent boundary layer in adverse pressure gradient. *J. Aero. Sci.*, 21:91–108, 1954.
17. S. J. Kline and F. A. McClintock. Describing uncertainties in single sample experiments. *Mech. Eng.*, 75(1):3–8, 1953.

18. H. H. Bruun. *Hot wire anemometry*. Oxford University Press, 1995.
19. M. Hultmark, S. C. C. Bailey, and A. J. Smits. Scaling of near-wall turbulence in pipe flow. *J. Fluid Mech.*, 649:103–113, 2010.
20. H .C. H. Ng, J. P. Monty, , M. S. Chong, and I Marusic. Comparison of turbulent channel and pipe flows with varying Reynolds number. *Exp. Fluids*, 51:1261–1281, 2011.
21. N. Hutchins, T. B. Nickels, I. Marusic, and M. S. Chong. Hot-wire spatial resolution issues in wall-bounded turbulence. *J. Fluid Mech.*, 635:103–136, 2009.
22. C. C. Chin, N. Hutchins, A. S. H. Ooi, and I. Marusic. Use of direct numerical simulation (DNS) data to investigate spatial resolution issues in measurements of wall-bounded turbulence. *Meas. Sci. Technol.*, 20:115401, 1–10, 2009.
23. P. E. Skåre and P.-Å. Krogstad. A turbulent equilibrium boundary layer near separation. *J. Fluid Mech.*, 272:319–348, 1994.
24. Y. Nagano and T. Houra. Higher-order moments and spectra of velocity fluctuations in adverse-pressure-gradient turbulent boundary layer. *Exp. Fluids*, 33:22–30, 2002.
25. D. Warnack and H. H. Fernholz. The effects of a favourable pressure gradient and of the Reynolds number on an incompressible axisymmetric turbulent boundary layer. Part 2. The boundary layer with relaminarization. *J. Fluid Mech.*, 359:357–381, 1998.
26. A. V. Johansson and P. H. Alfredsson. Effects of imperfect spatial resolution on measurements of wall-bounded turbulent shear flows. *J. Fluid Mech.*, 137:409–421, 1983.
27. P. Schlatter and R. Örlü. Quantifying the interaction between large and small scales in wall-bounded turbulent flows: A note of caution. *Phys. Fluids*, 22:051704, 1–4, 2010.
28. R. Mathis, N. Hutchins, and I. Marusic. Relationship between turbulence modulation and skewness in wall bounded flows. *In Proc. 7^{th} Turbulence and Shear Flow Phenomena, (TSFP). Ottawa, Canada*, 2011.
29. R. Mathis, N. Hutchins, I. Marusic, and K. R. Sreenivasan. The relationship between the velocity skewness and the amplitude modulation of the small scale by the large scale in turbulent boundary layers. *Phys. Fluids*, 23:121702, 1–4, 2011.
30. P.-Å. Krogstad and P. E. Skåre. Influence of a strong adverse pressure gradient on the turbulent structure in a boundary layer. *Phys. Fluids*, 7:2014–2024, 1995.